A Dual BEM Genetic Algorithm Scheme for the Identification of Polarization Curves of Buried Slender Structures

L.A. de Lacerda[1] and J. M. da Silva[1]

Abstract: A two-dimensional boundary element formulation is presented and coupled to a genetic algorithm to identify polarization curves of buried slender structures. The dual boundary element method is implemented to model the cathodic protection of the metallic body and the genetic algorithm is employed to deal with the inverse problem of determining the non-linear polarization curve, which describes the relation between current density and electrochemical potential at the soil metal interface. In this work, this non-linear relation resulting from anodic and cathodic reactions is represented by a classical seven parameters expression. Stratified soil resistivity is modeled with a piece-wise homogeneous domain. The inverse analysis is guided by potential measurements at the soil free surface. The identification method is analysed under different measurement conditions.

keyword: Dual boundary element method, Cathodic protection, Genetic algorithm, Inverse analysis.

1 Introduction

Corrosion in soil is a complex topic and the development of effective techniques for the protection of buried metallic structures is one of the main concerns of corrosion engineers.

Cathodic Protection (CP) is a technique, which uses the electrochemical properties of the metal to protect it. In order to have effective CP systems, it is necessary to have the metallic structure working as the cathode of an electrolytic cell. In high resistivity soils, impressed current systems are necessary to reduce the metal electric potential to values lower than a critical one, guaranteeing the cathodic behavior of the structure.

The boundary element method has been used to simulate cathodic protection of pipelines and offshore structures for more than a decade [Telles et al (1990); Yan et al (1992); Brichau and Deconinck (1994); Aoki et al (2004)]. The method is quite attractive for this type of analyses, since they involve unbounded half-space domains. Despite the medium heterogeneity, non-linearities are normally restricted to the soil – metal interfaces characterized by the polarization curves.

Recently, Lacerda et al. (2004) developed a two-dimensional boundary element formulation for the analysis of buried slender structures. This type of structure is normally found in foundations of electric transmission line towers. In many cases, frequently due to economical reasons, these metallic foundations are directly buried in the ground, which can be an aggressive environment depending on its properties.

Normally, the foundations are composed by a series of connected slender pieces forming a truss structure. The slenderness of the bodies brings some difficulties into the classical boundary element method, such as near singular integration and ill-conditioned systems, and to avoid this problem the dual boundary element method was implemented. The implementation included a Newton-Raphson solution algorithm for the non-linear boundary conditions and a piece-wise homogeneous layered half-space to model soil resistivity. They carried out a field experiment where a galvanized metallic sheet was buried alongside two Copper anodes, in parallel.

To design a CP system it is necessary to know the non-linear boundary condition or polarization curve of the structure. However, one of the main difficulties during field tests is to retrieve this condition. The usual process for obtaining it is slow and not very accurate since it is heavily dependent on the reader skills and patience. With this problem in mind an inverse analysis procedure is proposed using Genetic Algorithm. This type of approach has been successfully performed with the boundary element method [Mustata et al (2000); Miltiadou and Wrobel (2002)]. In this work, its performance is evaluated when the Dual formulation is used and random errors are introduced.

[1] LACTEC, Curitiba, PR, BRAZIL.

2   Half-space Dual Boundary Element Method

In the absence of volume forces, potential and current density boundary integral equations are given by [Wrobel (2002)],

$$c(\xi)\phi(\xi) = \int_{\Gamma} \phi^*(\xi,x)i(x)d\Gamma(x) - \int_{\Gamma} i^*(\xi,x)\phi(x)d\Gamma(x)$$

(1)

$$d(\xi)i(\xi) = \int_{\Gamma} \frac{\partial\phi^*(\xi,x)}{\partial n(\xi)}i(x)d\Gamma(x) - \int_{\Gamma} \frac{\partial i^*(\xi,x)}{\partial n(\xi)}\phi(x)d\Gamma(x)$$

(2)

where $\phi^*(\xi,x)$ and $i^*(\xi,x)$ are the potential and current density fundamental solutions at the field point x due to a unit source applied in ξ, the coefficients $c(\xi)$ and $d(\xi)$ are dependent on the geometry at ξ, $n(\xi)$ is the normal direction at ξ and $\phi(x)$ and $i(x)$ are the potential and current density at the boundary Γ. In Eq.2, a free term dependent on the continuity of the curvature at the collocation point is being omitted for simplicity. The fundamental solution expressions and its normal derivatives are given by,

$$\phi^*(\xi,x) = \frac{-1}{2k\pi}\ln(r)$$

(3)

$$i^*(\xi,x) = \frac{-1}{2\pi r}\frac{\partial r}{\partial n(x)}$$

(4)

$$\frac{\partial\phi^*(\xi,x)}{\partial n(\xi)} = \frac{-1}{2k\pi r}\frac{\partial r}{\partial n(\xi)}$$

(5)

$$\frac{\partial i^*(\xi,x)}{\partial n(\xi)} = \frac{1}{2\pi r^2}\left[n_j(x)n_j(\xi) + 2\frac{\partial r}{\partial n(x)}\frac{\partial r}{\partial n(\xi)}\right]$$

(6)

where r is the distance between the points x and ξ.

The classical boundary element method is developed from Eq.1. When slender bodies take part in the problem some difficulties may arise in the classical formulation, such as near-singular integrations and the assembling of ill-conditioned system of equations. The first problem becomes more pronounced with the growth of the ratio between the length of the discretizing boundary elements of the slender structure and its thickness. These problems can be avoided by using the dual formulation of the boundary element method. For this purpose, after the boundary discretization, it is necessary to apply the hypersingular boundary integral Eq.2 and the classical boundary integral Eq.1 to the nodes of the slender body, one at each side of the body.

The singularity of the current density fundamental solution derivative behaves like $O(1/r^2)$ and the second integral on the right hand side of Eq.2 must be interpreted in the Hadamard Principal Value sense.

Many of the cathodic protection problems involve an exterior domain, such as the case of buried structures. In problems of this type, Eqs.1 and 2 can be seen as,

$$c(\xi)\phi(\xi) = \int_{\Gamma} (\phi^*(\xi,x)i(x) - i^*(\xi,x)\phi(x))d\Gamma(x)$$

$$+ \int_{\Gamma_\infty} (\phi^*(\xi,x)i(x) - i^*(\xi,x)\phi(x))d\Gamma(x)$$

(7)

$$d(\xi)i(\xi) = \int_{\Gamma} \left(\frac{\partial\phi^*(\xi,x)}{\partial n(\xi)}i(x) - \frac{\partial i^*(\xi,x)}{\partial n(\xi)}\phi(x)\right)d\Gamma(x)$$

$$+ \int_{\Gamma_\infty} \left(\frac{\partial\phi^*(\xi,x)}{\partial n(\xi)}i(x) - \frac{\partial i^*(\xi,x)}{\partial n(\xi)}\phi(x)\right)d\Gamma(x)$$

(8)

where Γ_∞ represents a fictitious boundary at the infinite. The regularity condition at infinity, in this problem, implies that the potential behaves as $ln(r)$ plus a constant ϕ_∞, and the potential boundary integral equation becomes,

$$c(\xi)\phi(\xi) = \int_{\Gamma} (\phi^*(\xi,x)i(x) - i^*(\xi,x)\phi(x))d\Gamma(x) + \phi_\infty$$ (9)

while the integral over Γ_∞ in Eq.8 is equal to zero and the current density integral equation remains the same. To include the extra unknown ϕ_∞ in the system of equations another equation is necessary, the charge conservation equation,

$$\int_{\Gamma} i(x)d\Gamma(x) = 0$$

(10)

In half-space domains it is interesting to change the fundamental solution in order to avoid discretizing the infinite horizontal free surface of the problem. If the current density can be considered zero at this surface, the boundary integral equations for this particular situation

are written like,

$$c(\xi)\phi(\xi) = \int_{\Gamma} (\phi^*(\xi,x)i(x) - i^*(\xi,x)\phi(x))d\Gamma(x)$$

$$- \int_{\Gamma_H} i^*(\xi,x)\phi(x)d\Gamma(x) + \phi_\infty \qquad (11)$$

and

$$d(\xi)i(\xi) = \int_{\Gamma} \left(\frac{\partial\phi^*(\xi,x)}{\partial n(\xi)}i(x) - \frac{\partial i^*(\xi,x)}{\partial n(\xi)}\phi(x) \right)d\Gamma(x)$$

$$- \int_{\Gamma_H} \frac{\partial i^*(\xi,x)}{\partial n(\xi)}\phi(x)d\Gamma(x) \qquad (12)$$

with Γ_H representing the horizontal free surface. Therefore, if the fundamental solution $\phi^*(\xi,x)$ can be chosen in such a way that $i^*(\xi,x)$ and $\partial i^*(\xi,x)/\partial n(\xi)$ are zero for any point x in this boundary, the integral in Γ_H disappears and the analysis involves only the discretization of the finite boundary Γ.

It is easy to see that a function represented by the sum of two unit sources located at opposite sides and the same distance from the boundary Γ_H is the sought Green's function for the potential boundary integral equation. This function is represented by,

$$\phi^*(\xi,x) = -\frac{1}{2k\pi}\ln(r) - \frac{1}{2k\pi}\ln(r^i) \qquad (13)$$

where r^i is the distance between the field point x and the image ξ^i of the collocation point ξ with respect to the boundary Γ_H. The normal derivative of this function is as follows,

$$i^*(\xi,x) = -\frac{1}{2\pi r}\frac{\partial r}{\partial n(x)} - \frac{1}{2\pi r^i}\frac{\partial r^i}{\partial n(x)} \qquad (14)$$

This procedure is commonly called method of images.

It is interesting to notice that for the hypersingular equation the normal derivatives must be taken with respect to both the collocation point and its image. In fact, Eq.12 is not adequate for the method of images as it has been obtained from the differentiation of Eq.1 with respect to the direction $n(\xi)$, only. The hypersingular equation must be derived from the classical one through the application of the differential operator, $\frac{\partial}{\partial n(\xi)}() + \frac{\partial}{\partial n(\xi^i)}()$ plus a limiting process. After some algebraic manipulation, the hypersingular boundary integral equation for the method of

images is written like,

$$d(\xi)i(\xi) = \int_{\Gamma} (G(\xi,x)i(x) - H(\xi,x)\phi(x))d\Gamma(x) \qquad (15)$$

where,

$$G(\xi,x) = -\frac{1}{2\pi r}\frac{\partial r}{\partial n(\xi)} - \frac{1}{2\pi r^i}\frac{\partial r^i}{\partial n(\xi^i)} \qquad (16)$$

$$H(\xi,x) = \frac{1}{2\pi r^2}\left[n_k(x)n_k(\xi) + 2\frac{\partial r}{\partial n(x)}\frac{\partial r}{\partial n(\xi)} \right]$$

$$+ \frac{1}{2\pi r^{i2}}\left[n_k(x)n_k(\xi^i) + 2\frac{\partial r^i}{\partial n(x)}\frac{\partial r^i}{\partial n(\xi^i)} \right] \qquad (17)$$

It can be verified that if the field point x is over the boundary Γ_H,

$$i^*(\xi,x) = H(\xi,x) = 0 \qquad (18)$$

3 Direct Analysis

3.1 Experiment data

A field experiment was performed to assess the developed numerical formulation. Fig. 1 sketches the experiment, were a galvanized metallic sheet 64 cm long, 45 cm wide with a thickness of 1 mm, was buried 15 cm from the free-surface of the ground, in parallel between two Copper anodes with the same length and diameter of 2 cm. The central positioning of the sheet between the anodes can be observed in Fig. 1.

Soil resistivity was evaluated with Wenner method [ASTM, 1984)]. After a series of measurements the average resistivity for each depth is listed in Tab. 1.

A graphical scheme was employed to characterize soil resistivity in a two-layer model [Kindermann and Campagnolo (1995)]. Resistivities of 121 and 8.13 Ωm were obtained for the top layer with thickness of 1.9 m and infinite bottom one, respectively.

3.2 Equations and mathematical expressions

Six months after the metallic sheet was buried, corrosion potential measurements were taken using a Copper–Copper Sulfate (Cu-CuSO$_4$) reference electrode. During the measurements, the reference electrode was placed every 50cm between the sheet and each anode. The measuring points can be seen in Fig. 1, along three parallel
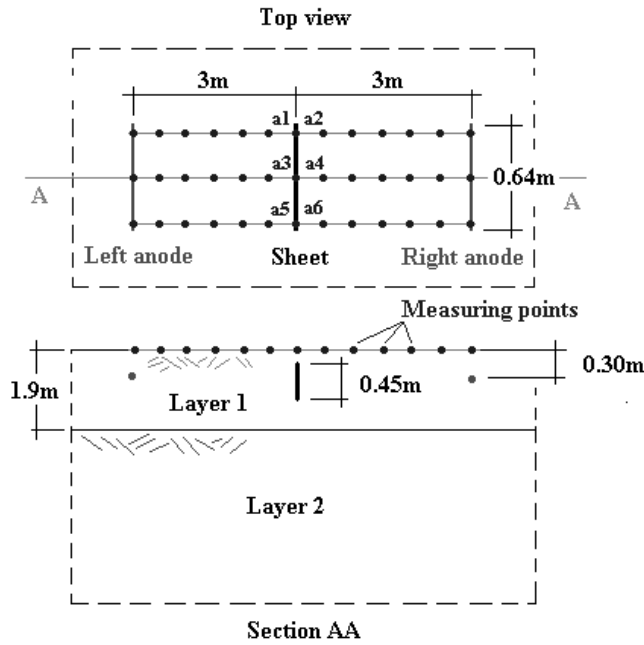
Figure 1 : Sketch of the field experiment: metallic sheet, anodes and measuring points.

Table 1 : Average soil resistivity in several depths.

Depth (m)	Resistivity (Ωm)
1.0	142.5
2.0	107.1
4.0	33.3
8.0	6.9
16.0	4.3

lines named a1, a3 and a5 on the left side and a2, a4 and a6 on the right side.

After a series of field measurements, the polarization curve data describing the relation between the current density (μA) and the electrochemical potential (mV) at the metallic sheet – soil interface were fitted by the equation [Yan et al (1992)],

$$i = e^{\frac{\phi - \phi_{Fe^{2+}}}{\beta_{Fe^{2+}}}} - \left(\frac{1}{i_{O_2}} + e^{\frac{\phi - \phi_{O_2}}{\beta_{O_2}}} \right)^{-1} - e^{\frac{-(\phi - \phi_{H_2})}{\beta_{H_2}}} \qquad (19)$$

where the equilibrium potentials, Tafel slopes and the current limit for oxygen reaction were, respectively,

given by

$$\phi_{Fe^{2+}} = -571mV; \phi_{O_2} = -580mV; \phi_{H_2} = -796mV;$$
$$\beta_{Fe^{2+}} = 20; \beta_{O_2} = 60; \beta_{H_2} = 80;$$
$$i_{O_2} = 19\mu A \qquad (20)$$

It is well known that the sheet boundary condition changes slowly in time. However, for the objectives of the present study conditions are considered static since the whole experiment is conducted in a short period of time.

3.3 Experimental and numerical results

Potential measurements on the ground surface between the metallic sheet and the anodes were taken when the current was injected into the ground through both anodes.

In the numerical analysis the soil was modeled in two layers accordingly to the soil characterization method. The bottom layer is a half-space domain with constant resistivity of 8.13 Ωm and bounded on the top by a 1.9 m layer of soil with higher resistivity. Since the method of images was employed only the interface between the two layers and the interface soil – metallic sheet were discretized. Fig. 2 shows a sketch of the analyzed model with the slender body, the current point sources and the layers interface.

The boundary condition at the metallic sheet (cathode) is represented by Eq.19. At the layers interface, potential continuity and current density equilibrium were imposed. At the top layer, different values of soil resistivity were tested and 100 Ωm provided a good fit between numerical and experimental results.

Fig. 3 shows a comparison between experimental and numerical results for three different current injections. Results are generally good and, as expected, differences tend to increase at points closer to the metallic sheet. These can be explained by two main reasons: the two-dimensional model is not perfectly representative for the dimensions of the experiment, and the capacitive behaviour of the metal-soil interface during current injections introduces undesired charges in the system in subsequent readings. Also, another source of errors is the adopted two-layer model.
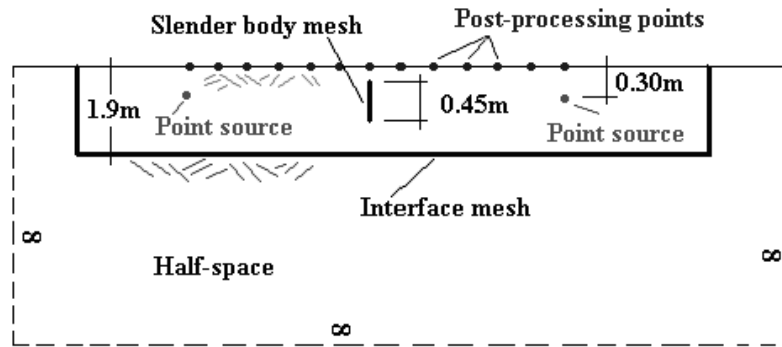
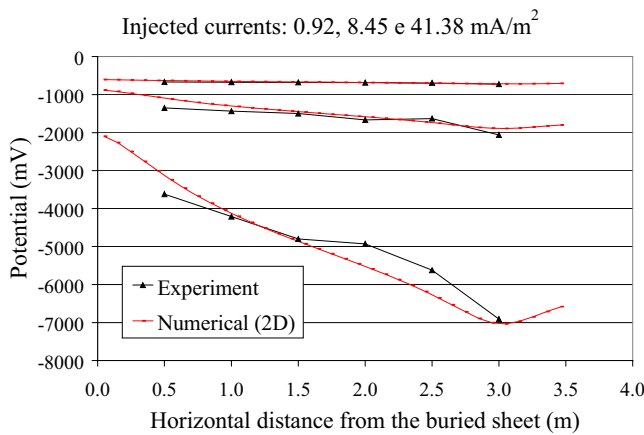**Figure 2** : Sketch of the analyzed boundary element model.

Figure 3 : Comparisons between experimental and numerical results.

4 Inverse Analysis

An inverse formulation is developed employing the genetic algorithm (GA) to identify the polarization curve in a test based on the previous experiment, via surface potential measurements. This type of analysis has been successfully performed by Miltiadou and Wrobel (2002). In this work, its performance is evaluated along with the Dual formulation.

In the numerical procedure, surface potential values are simple internal points computations, which involve only regular integral evaluations.

4.1 Genetic Algorithm

GA is a search technique, which emulates the process of evolution via survival of the fittest. Compared to other techniques, it presents interesting features such as no need for derivative evaluations and a higher likelihood of finding the global minimum [Goldberg (1989)].

The algorithm starts with an initial population formed by a random sample of individuals. Each individual in the population is formed by a group of parameters, which compose a problem solution. In this work, these parameters are listed in Eq.20. Each parameter is seen as chromosome or a bit string, and is bounded by limiting estimated values. The individual or group of chromosomes represents a possible solution to the problem, and its binary length is defined by the required precision for each parameter.

The implemented algorithm includes: tournament selection with a shuffling technique for choosing random pairs of individuals for mating, uniform crossover, jump mutation and elitism [Miltiadou and Wrobel (2002)].

4.2 Polarization curve parameters and GA control data

The inverse formulation was verified using potential surface results from a direct analysis with the polarization curve defined in Eqs.19 and 20. The group of surface values represents the "measurements" which are used to drive the GA. Each individual of the population provides a group of surface results, which is compared to the known "measurements". The minimization of this difference is the aim of the algorithm and the value of the difference is an indication of the individual's fitness.

On the search for the fittest individual, limits must be established for each parameter. Tab. 2 presents the estimated upper and lower limits for each one as well as the adopted precision.

After testing several sizes for the population, 20 individuals were found to be an adequate number, considering speed of convergence and precision. Probability of

Table 2 : Adopted limits for the polarization curve parameters.

| Parameter	Lower limit	Upper limit	Precision
$\phi_{Fe^{2+}}$	*-981 mV*	*-346 mV*	*5 mV*
ϕ_{O_2}	*-980 mV*	*-345 mV*	*5 mV*
ϕ_{H_2}	*-981 mV*	*-346 mV*	*5 mV*
$\beta_{Fe^{2+}}$	18	81	1
β_{O_2}	18	81	1
β_{H_2}	10	136	2
i_{O_2}	*10 mA*	*73 mA*	*1 mA*

crossover and mutation were fixed to 50% and 2%, respectively. A generation cycle is defined to comprehend individual fitness evaluations, mating and new population definition. In all analyses, the number of generations was limited to 100.

4.3 Identification of Polarization Curves

Since the objective of this analysis is to identify an existing non-linear relation between the electrochemical potential and the current density at the soil-metal interface, it is necessary to have measurements taken at several impressed current values.

For every impressed current, surface potential values were obtained at six points between the metallic sheet and the anode. Fig. 4 shows the influence of the number of impressed currents on the resulting polarization curve. The solid line is the relation used to generate the known "measurements". This is the relation being sought in this inverse analysis. The other lines in Fig. 4 are all results and each one is identified by a couple of numbers: the first one indicates the number of impressed currents and the second one, between brackets, indicates the generation when final convergence was achieved. As it can be seen, if only two impressed currents are used the non-linear boundary condition is represented by a straight line, as expected. The increasing number of impressed currents improves the final result of the inverse analysis. Observe that the polarization curve obtained when 10 impressed currents were used is in very close agreement to the original one. The number of generations when the final solution was found in each analysis does not seem to be correlated by the number of impressed currents.

The next set of results shows the influence of surface measurement errors on the results of the inverse analy-
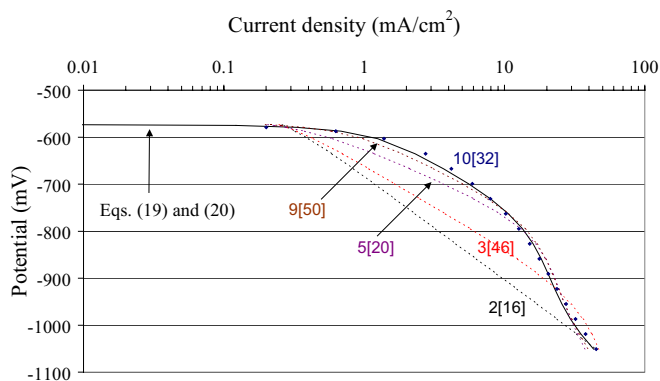
Figure 4 : Influence on the number of impressed currents: 2, 3, 5, 9 and 10. The impressed values were 0.1, 0.25, 5.25, 10.25, 15.25, 20.25, 25.25, 30.25, 35.25 and 40.25 $\mu A/cm^2$.
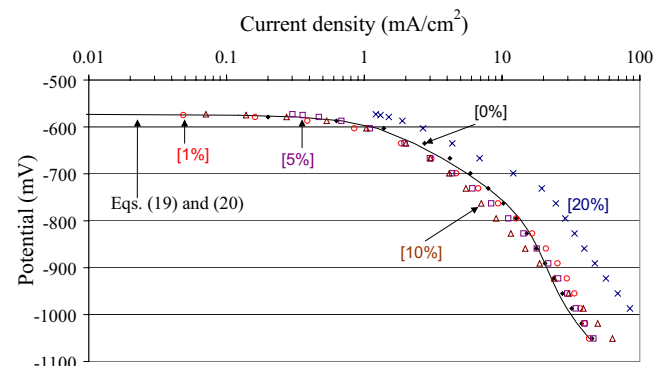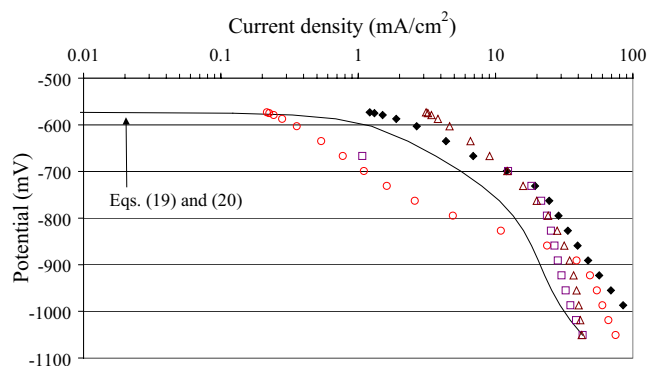

Figure 5 : Influence of surface measurement random errors: ± 0%, 1%, 5%, 10% and 20%.

sis. Random errors of ± 0%, 1%, 5%, 10% and 20% were applied to the measurements and the obtained polarization curves are shown in Fig. 5.

Each result is indicated between brackets and overall, results were good in all cases, apart from the 20% error oscillation condition. The potential differences between each obtained curve and the reference solid curve must be seen along a vertical line. For instance, from a visual inspection it can be seen that the relative error for the [20%] curve with respect to the reference curve is not greater than 20% at any point.

Fig. 6 shows a similar type of results for four different analyses with only ± 20% random errors. Notice that the randomness of the input data produces different sorts of results, which can be above, below or crossing the sought polarization curve.

Figure 6 : Influence of surface measurement random errors – Four analyses with $\pm$ 20% random errors.

It is important to point out that no input data regularization was applied and there is certainly room for some improvements.

5   Conclusions

A dual boundary element method for the analysis of two-dimensional cathodic protection of buried slender bodies has been developed and coupled to a genetic algorithm for the identification of polarization curves.

Details about the derivation of the hypersingular equation to be used with the method of images were presented. Its implementation along with the classical equation included the following characteristics which were used in all analyses: the additional equation of charge conservation for infinite and half-space domains; subregions for layered domains with different properties and a Newton-Raphson solution algorithm for the non-linear boundary conditions representing the polarization curves.

An experimental test was executed to retrieve the polarization curve of a buried slender metallic sheet as well as surface potential measurements. The Dual BEM model was verified considering a two-layer soil resistivity stratification.

The inverse analysis tests with the genetic algorithm showed that the developed method is capable of identifying the polarization curve from simple surface measurements. Different measurement conditions were introduced in the input data and the whole procedure was always convergent, providing results with errors, which were comparable to the inserted ones.

References

Aoki, S.; Amaya, K.; Urago, M.; Nakayama, A. (2004): Fast Multipole Boundary Element Analysis of corrosion Problems. *CMES: Computer Modeling in Engineering & Science*, Vol. 6, pp. 123-132

ASTM (1984): *Standard method for field measurements of soil resistivity using the Wenner four electrodes method*. G57-7.

Brichau, F.; Deconinck, J. (1994): A numerical model for cathodic protection of buried pipes, *Corrosion* , vol. 50(1), pp. 39-49.

Goldberg, D.E. (1989): *Genetic Algorithms in Search, Optimization and Machine Learning*, Addison-Wesley.

Kindermann, G.; Campagnolo, J. M. (1995): *Aterramento Elétrico*. Sagra-DC-Luzzato: Porto Alegre; 1-214.

Lacerda, L. A.; Oliveira, P. A.; Lázaris, J.; Silva, J. M. (2004): Analysis of a 2D cathodic protection system for a buried slender structure with the dual boundary element method. In: *ECCOMAS 2004 - European Congress on Computational Methods in Applied Sciences and Engineering*, Jyväskylä, Finland.

Mustata, R.; Harris, S.D.; Elliott, L.; Lesnic, D.; Ingham, D.B. (2000): An Inverse Boundary Element Method for Determining the Hydraulic Conductivity in Anisotropic Rocks. *CMES: Computer Modeling in Engineering & Science*, Vol. 1, pp 107-116.

Miltiadou, P.; Wrobel, L. C. (2002): A BEM-Based Genetic Algorithm for Identification of Polarization Curves in Cathodic Protection Systems, *International Journal for Numerical Methods in Engineering*, vol. 54(2), pp. 159-174.

Telles, J. C. F.; Mansur, W. J.; Wrobel, L. C.; Marinho, M. G. (1990): Numerical simulation of cathodically protected semisubmersible platform using the PROCAT system. *Corrosion*, vol. 46, pp. 513-518.

Wrobel, L. C. (2002): *The Boundary Element Method*, Wiley: Chichester, London.

Yan, J. F.; Pakalapati, S. N. R.; Nguyen, T. V.; White, R. E.; Grifin, R. B. (1992): Mathematical Modeling of Cathodic Protection Using the Boundary Element

Method with a Nonlinear Polarization Curve. *Journal of the Electrochemical Society*, vol. 139(7), pp. 1932-1936.